AIAA 2000-0452

Magnetic Control of Hypersonic Blunt Body Flow

J. Poggie D. V. Gaitonde
US Air Force Research Laboratory
Wright-Patterson AFB, OH 45433-7521

38th Aerospace Sciences Meeting & Exhibit
10-13 January 2000/Reno, NV

Magnetic Control
of Hypersonic Blunt Body Flow

J. Poggie[*]

D. V. Gaitonde[†]

US Air Force Research Laboratory

Wright-Patterson AFB, OH 45433-7521

The possibility of magnetic control of hypersonic blunt body flows was explored theoretically and computationally. A theoretical model, developed by W. B. Bush, of hypersonic flow over an axisymmetric, spherical-nose body with an imposed dipole field was reviewed. A preliminary computational study of the flow over a two-dimensional cylinder configuration with magnetic control was carried out employing a new, non-ideal, magnetogasdynamics code. Using an inviscid model for the outer flow, both the theory and the computations show than an applied magnetic field can slow the flow in the shock layer. Boundary layer theory predicts a reduction in the stagnation point heat transfer. The effectiveness of control was found to be sensitive to the electrical conductivity of the ionized air in the shock layer. Magnetic field strengths on the order of 1 T (10^4 G) or higher are needed for electrical conductivities corresponding to the natural levels of ionization present in typical re-entry flows ($\sim 10^2/(\Omega\text{-m})$). Higher conductivity allows correspondingly lower magnetic field strengths to achieve the same level of control. More uniform conductivity also improves the effectiveness of magnetic control, and mitigates the tendency of the stagnation point boundary layer to develop overshoot velocity profiles.

Nomenclature

Roman Symbols

$\vec{B}$	= magnetic field
$\mathbf{C}$	= total stress tensor
C	= a constant
C_p	= constant pressure specific heat
C_f	= skin friction coefficient
C_h	= heat transfer coefficient
$\vec{E}$	= electric field
$\vec{f}$	= body force
$F(r)$	= velocity similarity function
G	= velocity gradient parameter
h	= enthalpy
$\vec{H}$	= total energy transport vector
$\mathbf{I}$	= identity tensor, components δ_{ij}
$\vec{J}$	= conduction current density
k	= thermal conductivity
K	= shock density ratio
m	= symmetry parameter
M	= Mach number
$M(r)$	= magnetic field similarity function
$\mathbf{M}$	= Maxwell stress tensor
n	= exponent in conductivity formula
p	= pressure
P	= power delivered by body forces to fluid
Pr	= Prandtl number, $\mu C_p/k$
$\vec{q}$	= heat flux
Q	= magnetic interaction parameter
$r(x)$	= body radius
r, θ, ϕ	= spherical coordinates
R	= radius
Re_m	= magnetic Reynolds number
$\vec{S}$	= Poynting vector, $\vec{E} \times \vec{B}/\mu_0$
t	= time
T	= temperature
u, v, w	= Cartesian velocity components
U	= magnetic field energy, $B^2/2\mu_0$
V	= fluid velocity
$\vec{v}$	= fluid velocity
x,y,z	= Cartesian coordinates
Z	= total energy of fluid and field

Greek Symbols

γ	= specific heat ratio
δ	= boundary layer thickness
δ_{ij}	= Kronecker delta
Δ	= shock standoff
η	= magnetic diffusivity, $1/\sigma\mu_0$
λ	= second viscosity coefficient
μ	= dynamic viscosity
μ_0	= permeability of vacuum
ξ, η	= boundary layer similarity variables
ρ	= density
σ	= electrical conductivity
τ	= shear stress tensor
τ_w	= magnitude of shear stress at wall
ψ	= stream function
$\vec{\omega}$	= vorticity

[*]Research Aerospace Engineer, Air Vehicles Directorate, AFRL/VAAC, 2210 Eighth Street. Senior Member AIAA.

[†]Research Aerospace Engineer, Air Vehicles Directorate, AFRL/VAAC, 2210 Eighth Street. Associate Fellow AIAA.

Introduction

GIVEN the high temperatures in the shock layer in hypersonic flight, and the concomitant electrical conductivity due to weak ionization, it is natural to consider whether an electromagnet fixed in the nose of a blunt body can be used to control the flow. Since the Lorentz force tends to oppose fluid motion across magnetic field lines, magnetic control would tend to increase the drag of a vehicle (a desirable effect for atmospheric entry), and, by slowing the flow near the surface of the body, reduce heat transfer and skin friction. (A magnetic field imposed upstream of the bow shock could, in principle, reduce the shock pressure ratio, but control by this means is not considered here.)

Interest in the electromagnetic control of hypersonic flows seems to have arisen independently among several research groups in the late 1950's. Kantrowitz[1] suggested this idea in an early paper, and Resler and Sears[2–4] reviewed the prospects of magnetogasdynamic control, including the use of magnetic drag on re-entry vehicles and the reduction of heat transfer and skin friction on a blunt body.

A relatively complete theory of hypersonic flow over a sphere with an imposed dipole field was developed by Bush.[5–9] The imposed field was found to increase shock standoff and reduce heat transfer to the nose of the sphere. The change in shock standoff was confirmed experimentally by Ziemer.[5,10]

Bush[5–7] modeled the inviscid outer flow using a modification of the constant density theory. It should be noted that Kemp[11–14] developed a very similar model at about the same time, but Ziemer and Bush[5] seem to have priority for a correct theoretical model and its experimental confirmation. Lykoudis[15] also developed an inviscid-flow model using a modification of the Newtonian theory.

Bush modeled the viscous flow near the body surface using boundary layer theory.[8,9] Earlier studies[16–20] considered the viscous stagnation point problem, but assumed constant property boundary layer flow and a fixed inviscid outer flow, which produced somewhat misleading results. Later work[11,13,14,21,22] pointed out the importance of the interaction of the inviscid and viscous portions of the stagnation point flow; Bush generalized these results.

Cambel et al.[23–26] carried out additional calculations and experiments on the magnetically-controlled hemisphere/cylinder configuration. In particular, they made detailed measurements of the increase in total drag and shock standoff, and compared them with available theory.

Wu et al.[27–31] considered the fully viscous shock layer problem. These calculations appear to have been controversial;[24,30] Nowak et al.[25] indicate that the change in shock standoff is diminished for low Reynolds numbers.

The Hall current was neglected in early studies; it tends to reduce the overall effect of magnetic control. Levy[32] showed with a simple example how this phenomenon reduces the force exerted on the flow by a given magnetic field. Porter and Cambel[33] extended Bush's inviscid-flow analysis to include the Hall effect, and found a significant reduction in the change in shock standoff and drag for a given applied magnetic field under atmospheric entry conditions. It may be possible, however, to exploit the Hall effect to produce rolling moments.[34]

A number of authors have considered the practical application of magnetic control. Goulard[35] pointed out that as the shock standoff distance is increased, the radiative heat transfer to the body may also increase, and that an optimum imposed magnetic field strength may exist that minimizes the heat transfer to the body. Phillips[36] considered the effect of magnetic drag on the total heat load of an aerospace vehicle during atmospheric entry, and concluded that a substantial benefit could be obtained from increased drag alone. Ericson and Maciulaitis[37] investigated the possibility of flight control using asymmetric magnetic forces.

More recent interest in electromagnetic flow control for hypersonic flight has arisen following the public disclosure of the Russian AJAX concept vehicle.[38] At least four physical mechanisms have been identified[39–41] that may explain the effects observed in plasma flow control experiments: aerodynamic effects of injected plasma (the jet spike concept), energy storage in thermodynamic nonequilibrium and its subsequent release, thermal inhomogeneity, and magnetogasdynamic effects. Aerodynamic effects,[41] thermal effects,[42,43] and nonequilibrium energy release[43–45] have been addressed in other studies by our research group. Here we address magnetogasdynamic effects. In particular, we examine the physics of magnetically-

decelerated hypersonic blunt body flow, using Bush's theoretical model and a recently-developed computer code[46] for three-dimensional, non-ideal magnetogasdynamics.

Physical Model

For the present work, we adopt a magnetogasdynamic (MGD) model of the weakly-ionized flow over an aerospace vehicle. Detailed discussion of the approximation of magnetogasdynamics is given in standard texts on magnetohydrodynamics[47] and plasma physics.[48] For an MGD model to apply, typical flow length scales must be larger than the Debye length, corresponding time scales must be larger than the reciprocal of the plasma frequency, and the speed of the fluid must be small compared to the speed of light.

Under these conditions, Maxwell's equations can be written as:

$$\nabla \cdot \vec{J} = 0 \tag{1}$$
$$\nabla \cdot \vec{B} = 0 \tag{2}$$
$$\nabla \times \vec{E} = -\partial \vec{B}/\partial t \tag{3}$$
$$\nabla \times \vec{B}/\mu_0 = \vec{J} \tag{4}$$

The force on the fluid is $\vec{f}_{em} = \vec{J} \times \vec{B}$ and the power delivered to the fluid is $P_{em} = \vec{E} \cdot \vec{J}$. The displacement current and the convected charge have been neglected as small compared to the conduction current. The unsteady term in the charge conservation equation and the force due to the electric field have also been neglected.

We assume that the current is given by Ohm's law:

$$\vec{J} = \sigma(\vec{E} + \vec{v} \times \vec{B}) \tag{5}$$

A scalar electrical conductivity is a good approximation if the collision frequency is much greater than the cyclotron (gyro) frequency, as in a relatively dense gas. Eqs. (1) to (5) can be combined to eliminate the electric field, giving the magnetic induction equation:

$$\frac{\partial \vec{B}}{\partial t} = \nabla \times (\vec{v} \times \vec{B} - \eta \nabla \times \vec{B}) \tag{6}$$

Conservation of mass, momentum, and energy can be expressed as:

$$\frac{\partial \rho}{\partial t} + \nabla \cdot (\rho \vec{v}) = 0 \tag{7}$$
$$\frac{\partial}{\partial t}(\rho \vec{v}) + \nabla \cdot (\rho \vec{v} \vec{v} - \mathbf{C}) = 0 \tag{8}$$
$$\frac{\partial Z}{\partial t} + \nabla \cdot (\vec{v} Z - \mathbf{C} \cdot \vec{v} + \vec{H}) = 0 \tag{9}$$

where we have introduced a total energy of the fluid and field together: $Z = \rho(e + v^2/2) + U$, a total stress tensor due to contact and body forces: $\mathbf{C} = -p\mathbf{I} + \tau + \mathbf{M}$, and a total energy transport vector due to heat

transfer and magnetic diffusion: $\vec{H} = \vec{q} + \eta \nabla \cdot \mathbf{M}$. The Maxwell stress tensor is:

$$M_{ij} = \frac{1}{\mu_0} B_i B_j - \frac{B^2}{2\mu_0} \delta_{ij} \tag{10}$$

Equations (8)-(9) express the conservation of momentum and energy for the fluid and field together, and contain no source terms. In the momentum equation an additional stress arises due to the magnetic body force. The rate of change of the magnetic field field energy appears in the energy conservation equation, along with an associated energy flux represented by the Poynting vector. The Poynting vector can, in turn, be separated into terms that are interpreted as an addition to the total energy, work done by the Maxwell stress, and an addition to the heat flux:

$$\vec{S} = U\vec{v} - \mathbf{M} \cdot \vec{v} + \eta \nabla \cdot \mathbf{M} \tag{11}$$

For viscous-flow calculations, we use the usual constitutive equations for the viscous stress and heat flux in a Newtonian fluid:

$$\tau_{ij} = \mu \left(\frac{\partial u_i}{\partial x_j} + \frac{\partial u_j}{\partial x_i} \right) + \lambda \frac{\partial u_k}{\partial x_k} \delta_{ij} \tag{12}$$
$$q_i = -k \frac{\partial T}{\partial x_i} \tag{13}$$

Viscosity was computed using the Sutherland formula for air, and we take $\lambda = -2\mu/3$. Prandtl number was taken as constant. For the analytical studies, electrical conductivity was taken as: $\sigma \propto T^n$, where the exponent is either $n = 4.1$ for a rough approximation for air, or $n = 0$ for constant conductivity. For the numerical effort, conductivity was assumed to be constant.

An ideal gas, with constant specific heats ($p = \rho RT$ and $p = (\gamma - 1)\rho e$), is assumed as a simple thermodynamic model to illustrate the basic flow physics without the additional complexity of chemically-reacting air. Reacting gas effects are being addressed in ongoing work.[44,45]

Theoretical Model

Here we review the theoretical model developed by Bush[6–9] for this problem. We assume that the Reynolds number is high enough that the flow can be divided into an inviscid outer flow and a viscous boundary layer.

Inviscid Flow

Bush[6,7] modeled the inviscid outer flow using a modification of the constant density theory originally applied to non-magnetic, hypersonic flows over spheres and cylinders.[49–53] The basic idea of the constant density theory is that, for a strong bow shock, the flow in the vicinity of the nose of a blunt body is effectively incompressible ($\nabla \cdot \vec{v} \approx 0$), since the Mach number in that region is very low.

A local solution is developed for the vicinity of the stagnation point, assuming constant density in that region. The major drawback of this approach is that the density ratio varies along the bow shock in a real blunt body flow, so that the flow is more realistically modeled as a stratified, rather than constant density, flow ($D\rho/Dt = 0$, rather than $\rho = \text{const}$). Nevertheless, the constant density theory gives a quite reasonable estimate of the shock standoff distance for large shock density ratios at the nose. At $\rho/\rho_\infty = 3$, for example, the standoff predicted by the non-magnetic constant density solution for a sphere[49–51] is within 15% of experimental data obtained in air,[54] and the agreement improves for stronger shocks.

We consider a steady, axisymmetric flow over a sphere, assuming that that the effects of viscosity and compressibility are negligible and that the electrical conductivity is constant within the shock layer. The freestream electrical conductivity is taken to be zero. We require that the azimuthal (ϕ) component of the magnetic field and of the fluid velocity be zero. In consequence, the electric current must flow only in the azimuthal direction, and the electric field must be zero.

We cast the equations in nondimensional form using the freestream velocity V_∞, the shock radius R_s, and a reference magnetic field strength $B_0 = B_{s0}/2$, where B_{s0} is the centerline magnetic field strength at the shock. With no electric field, Maxwell's equations reduce to:

$$\nabla \cdot \vec{B} = 0 \tag{14}$$
$$\nabla \times \vec{B} = \text{Re}_m\, \vec{v} \times \vec{B} \tag{15}$$

For the constant density flow in the shock layer, the continuity equation and the vorticity transport equation (curl of the momentum equation) become:

$$\nabla \cdot \vec{v} = 0 \tag{16}$$
$$\nabla \times (\vec{\omega} \times \vec{v}) = \frac{Q}{K}\nabla \times [(\vec{v} \times \vec{B}) \times \vec{B}] \tag{17}$$

where the only non-zero component of vorticity is in the ϕ-direction: $\vec{\omega} = \omega\hat{e}_\phi$. We have introduced the nondimensional parameters: $Q = \sigma B_0^2 R_s/\rho_\infty V_\infty$, $K = \rho/\rho_\infty$, and $\text{Re}_m = \sigma\mu_0 R_s V_\infty$.

Here we consider the inverse problem, specifying a spherical shock and solving for the corresponding body, which is also a sphere for a reasonable range of flow conditions. To solve the problem, we write Eqs. (14)-(17) in spherical coordinates, impose inflow boundary conditions at the downstream side of the shock, and march the solution downstream until inviscid wall conditions are satisfied, indicating the location of the body surface. We take the imposed magnetic field to be a dipole located at the center of the sphere, and solve for the induced field. Figure 1 is a schematic diagram of the configuration. Note that $x = r\cos\phi\sin\theta$, $y = r\sin\phi\sin\theta$, and $z = r\cos\theta$,
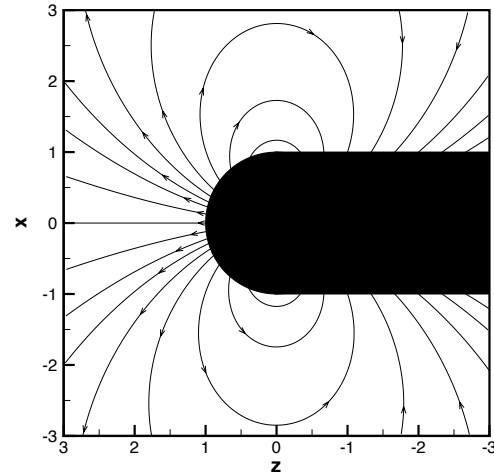

Fig. 1 Schematic diagram of blunt body with imposed magnetic field.

where the z-axis is directed opposite the freestream flow.

For a non-zero magnetic Reynolds number, the boundary conditions on the magnetic field require careful treatment.[24] If we assume that both the freestream and the body consist of non-conducting and non-magnetic material, then the magnetic field must satisfy a Laplace equation in these regions. With the symmetry assumed in the present problem, the solution for both regions has the form of a dipole. We require that the magnetic field approach zero far away from the body, so the nondimensional freestream field becomes:

$$\vec{B} = \frac{2\cos\theta}{r^3}\hat{e}_r + \frac{\sin\theta}{r^3}\hat{e}_\theta \tag{18}$$

This equation, evaluated just downstream of the shock ($r = 1$), provides an initial condition for the downstream-marching solution. Similarly, the nondimensional field inside the body has the form:

$$\vec{B} = \left(\frac{B_{g0}}{B_0}\frac{r_b^3}{r^3} + C\right)\cos\theta\,\hat{e}_r +$$
$$\left(\frac{B_{g0}}{B_0}\frac{r_b^3}{2r^3} - C\right)\sin\theta\,\hat{e}_\theta \tag{19}$$

where C is a constant related to the distortion of the imposed dipole field by the flow, and B_{g0} is the field intensity at the nose of the body in the absence of flow. Once the solution has been marched from the shock to the body, we can determine the magnetic field strengths at the nose of the body in flight (B_{b0}) and on the ground (B_{g0}) that correspond to the field at the shock (B_{s0}).

Another set of boundary conditions is provided by the velocity and vorticity just downstream of the shock. In the limit of small conductivity considered by Bush, the magnetic field does not have a

direct effect on the shock jump conditions. (This is not the case in the infinite conductivity limit.[55]) Using mass conservation across the shock, we find that the nondimensional radial velocity component is $v_r(1,\theta) = -\cos\theta/K$. The tangential velocity is continuous across the shock, so $v_\theta(1,\theta) = \sin\theta$. The vorticity just downstream of the shock is a function of the shock curvature, the density ratio, and and the tangential component of the Lorentz force.[27] In the present problem, the nondimensional vorticity just downstream of the shock can be expressed as follows:

$$\omega_\phi = \frac{(K-1)^2}{K}\sin\theta + 4Q\left(1+\frac{1}{2K}\right)\sin\theta\cos\theta \quad (20)$$

Assuming a stream function of the form $\psi = F(r)\sin^2\theta$, we obtain:

$$\vec{v} = [2F(r)\cos\theta/r^2]\hat{e}_r + [-F'(r)\sin\theta/r]\hat{e}_\theta \quad (21)$$

This form satisfies Eq. (16) and is consistent with the velocity boundary conditions at the shock. Similarly, a function of the form $M(r)\sin^2\theta$ satisfies Eq. (14) and the boundary conditions at the shock. The magnetic field becomes:

$$\vec{B} = [2M(r)\cos\theta/r^2]\hat{e}_r + [-M'(r)\sin\theta/r]\hat{e}_\theta \quad (22)$$

Substituting Eqs. (21) and (22) into Eqs. (17) and (15), we find that a θ-dependence remains, unless we use the small angle approximations $\sin\theta \approx \theta$ and $\cos\theta \approx 1$ for the trigonometric functions.

Under these conditions, the vorticity transport and induction equations become:

$$F''' - \frac{2}{r}F'' - \frac{2}{r^2}F' + \frac{8}{r^3}F = \quad (23)$$
$$-\frac{Q}{K}\frac{2}{r^2}\frac{M}{F}\left[F''M - FM'' - \frac{4}{r}F'M + \frac{4}{r}FM'\right]$$

and

$$M'' - \frac{2}{r^2}M = -\text{Re}_m\frac{2}{r^2}(-FM' + F'M) \quad (24)$$

with the boundary conditions:

$$F(1) = -1/2K \quad (25)$$
$$F'(1) = -1 \quad (26)$$
$$F''(1) = -K + 2(1 - 1/K)$$
$$\qquad\quad -4Q(1 + 1/2K) \quad (27)$$
$$M(1) = 1 \quad (28)$$
$$M'(1) = -1 \quad (29)$$

The solution must be marched to the body surface $r = r_b$ such that:

$$\lim_{r \to r_b} F(r) = 0 \quad (30)$$

Matching Eqs. (19) and (22) at the body surface gives:

$$\frac{B_{g0}}{B_0} = \frac{4M(r_b)}{3r_b^2} - \frac{2M'(r_b)}{3r_b} \quad (31)$$
$$\frac{B_{t0}}{B_0} = \frac{2M(r_b)}{r_b^2} \quad (32)$$

We define parameters, analogous to Q and Re_m, that only depend on information known before solving the problem: $Q_g = \sigma B_{g0}^2 R_b/\rho_\infty V_\infty$, and $\text{Re}_m^* = \sigma\mu_0 R_b V_\infty$. With the solution known, the two forms of the interaction parameter and the magnetic Reynolds number can be related: $Q_g = Qr_b(B_{g0}/B_0)^2$ and $\text{Re}_m^* = r_b\text{Re}_m$

The nondimensional stagnation point velocity gradient is given by:

$$\left(\frac{1}{r}\frac{\partial v_\theta}{\partial\theta}\right)_b = -\frac{F'(r_b)}{r_b^2} \quad (33)$$

The nondimensional pressure gradient along the body surface is given by:

$$\left(\frac{1}{r}\frac{\partial p}{\partial\theta}\right)_b = \left[\frac{4Q[M(r_b)]^2F'(r_b)}{r_b^5} - \frac{K[F'(r_b)]^2}{r_b^3}\right]\theta \quad (34)$$

The inviscid-flow Eqs. (23)-(24) were integrated using an adaptive Runge-Kutta-Fehlberg 4-5 method, from the initial conditions, Eqs. (25)-(29), until Eq. (30) was satisfied. Calculations were carried out for a fixed Q_g and Re_m^*; iteration was used to find the corresponding values of Q and Re_m.

Viscous Boundary Layer

Following Bush,[8,9] we examine the flow near the wall using laminar boundary layer theory. If we assume that there are no electrodes to introduce a potential difference, then it is valid to take the electric field as zero in steady flow. We assume that current only flows in the transverse direction, and that there is no fluid flow in that direction. Making the usual assumptions of boundary layer theory, we can show that only the wall-normal component of the magnetic field has a significant influence on the boundary layer flow. We use an orthogonal, curvilinear coordinate system (x, y, z) with the origin at the stagnation point, and $y = 0$ on the body surface.

In the MGD boundary layer approximation, the equation for conservation of mass is:

$$\frac{\partial}{\partial x}(\rho u r^m) + \frac{\partial}{\partial y}(\rho v r^m) = 0 \quad (35)$$

where $r(x)$ is the body radius, and $m = 0$ for planar symmetry and $m = 1$ for axial symmetry. The conservation of momentum is expressed as:

$$\rho u\frac{\partial u}{\partial x} + \rho v\frac{\partial u}{\partial y} = -\frac{dp}{dx} + \frac{\partial}{\partial y}\left(\mu\frac{\partial u}{\partial y}\right) - \sigma B_y^2 u \quad (36)$$

where $B_y = B_y(x)$. Note that the magnetic force will tend to oppose the flow, no matter what the sign of B_y. In the freestream, the momentum equation reduces to:

$$\frac{dp}{dx} = -\left(\rho_e u_e \frac{du_e}{dx} + \sigma_e B_y^2 u_e\right) \tag{37}$$

For a uniform freestream velocity and non-zero conductivity in the freestream, a favorable pressure gradient must exist to balance the magnetic retarding force. In general, the magnetic force slows the flow within the boundary layer, but the pressure gradient set up by the effect of magnetic forces on the freestream can accelerate the flow.

The conservation of energy has the form:

$$\rho u \frac{\partial h}{\partial x} + \rho v \frac{\partial h}{\partial y} = u\frac{dp}{dx} + \tag{38}$$
$$\frac{\partial}{\partial y}\left(k\frac{\partial T}{\partial y}\right) + \mu\left(\frac{\partial u}{\partial y}\right)^2 + \sigma B_y^2 u^2$$

The boundary conditions at the wall are no slip and no temperature jump. At the boundary layer edge, the solution must match the inviscid outer flow.

For an axisymmetric stagnation point boundary layer, $m = 1$, $r = x$, and $u_e = Gx$, where $G = (du_e/dx)_0$ is constant. For a uniform magnetic field ($B_y = B_{b0}$), a similarity solution can be obtained with the introduction of the following variables:

$$\xi(x) = \frac{1}{2(m+1)}\rho_e \mu_e G x^{2(m+1)} \tag{39}$$

$$\eta(x,y) = \sqrt{\frac{(m+1)G}{\rho_e \mu_e}}\int_0^y \rho d\hat{y} \tag{40}$$

We look for solutions of the form: $u = u_e(\xi)f'(\eta)$ and $h = h_e(\xi)g(\eta)$. Once the solution is known, the transformation can be inverted using the following equation:

$$y\sqrt{\rho_e G/\mu_e} = \sqrt{\frac{1}{m+1}}\int_0^\eta P^{-1}d\hat{\eta} \tag{41}$$

We introduce an interaction parameter $Q_v = \sigma_e B_{b0}^2/\rho_e G$, and a nondimensional conductivity $\sigma^* = \sigma/\sigma_e$. (Note that $Q_g = KG^*Q_v(B_{g0}/B_{b0})^2$, where $G^* = GR_b/V_\infty$.) The momentum equation becomes:

$$(Cf'')' + ff'' + \tag{42}$$
$$\frac{1}{m+1}\left\{P^{-1}\left[1 + Q_v\left(1 - \sigma^* f'\right)\right] - f'^2\right\} = 0$$

The enthalpy equation is:

$$\left(\frac{C}{Pr}g'\right)' + fg' = 0 \tag{43}$$

The terms in Eq. (38) representing the effects of the pressure gradient, viscous dissipation, and Joule heating are negligible here due to the low flow speed in the stagnation point region.

The velocity boundary conditions are: $f(0) = 0$, $f'(0) = 0$, and $f'(\infty) = 1$. The corresponding conditions on the enthalpy are: $g(0) = g_w$ and $g(\infty) = 1$.

With the solution known, the skin friction and wall heat transfer can be found from:

$$C_f = \sqrt{m+1}f''(0)C_w \tag{44}$$

$$C_h = \frac{\sqrt{m+1}g'(0)}{1-g(0)}\frac{C_w}{Pr_w} \tag{45}$$

where

$$C_f = \frac{\tau_w}{u_e\sqrt{\rho_e \mu_e G}} \tag{46}$$

$$C_h = \frac{q_w}{(h_w - h_e)\sqrt{\rho_e \mu_e G}} \tag{47}$$

The shear stress and heat flux relative to the non-magnetic case are given by:

$$\frac{\tau_{w,m}}{\tau_{w,nm}} = \left(\frac{G_m}{G_{nm}}\right)^{3/2}\frac{C_{f,m}}{C_{f,nm}} \tag{48}$$

$$\frac{q_{w,m}}{q_{w,nm}} = \left(\frac{G_m}{G_{nm}}\right)^{1/2}\frac{C_{h,m}}{C_{h,nm}} \tag{49}$$

Boundary layer calculations were carried out, for conditions corresponding to the inviscid flows found by solving Eqs. (23)-(24). The boundary layer equations, (42)-(43), were also integrated, using the adaptive Runge-Kutta-Fehlberg 4-5 method. The boundary conditions were satisfied by a shooting scheme based on Newton-Raphson iteration.

Example Calculations

As an example, consider an aerospace vehicle of 1 m nose radius, flying at an altitude of 61 km at a Mach number of 25. The pressure and temperature at this altitude in the standard atmosphere are about 180 Pa and 250 K, respectively. The corresponding velocity is about 8 km/s.

If we assume that chemical equilibrium exists downstream of the bow shock at the nose of the body, the density ratio across the shock is $K = 15.8$. The electrical conductivity, based on a simple model for air,[56] is roughly $\sigma = 300/\Omega$-m ($Re_m^* = 3.01$).

(It should be noted that the Hall effect is expected to be important under these conditions,[33] and will tend to reduce the efficiency of the control scheme. The present example should be interpreted as giving an upper limit on the effectiveness of magnetic control in the absence of artificial ionization used to increase the electrical conductivity.)

Figure 2 shows contours of the nondimensional streamfunction for the inviscid outer flow. Corresponding streamlines are added in the freestream for completeness. The upper plot, Fig. 2a, shows the case with no applied magnetic field; the results agree well with the analytical solutions of Hida and
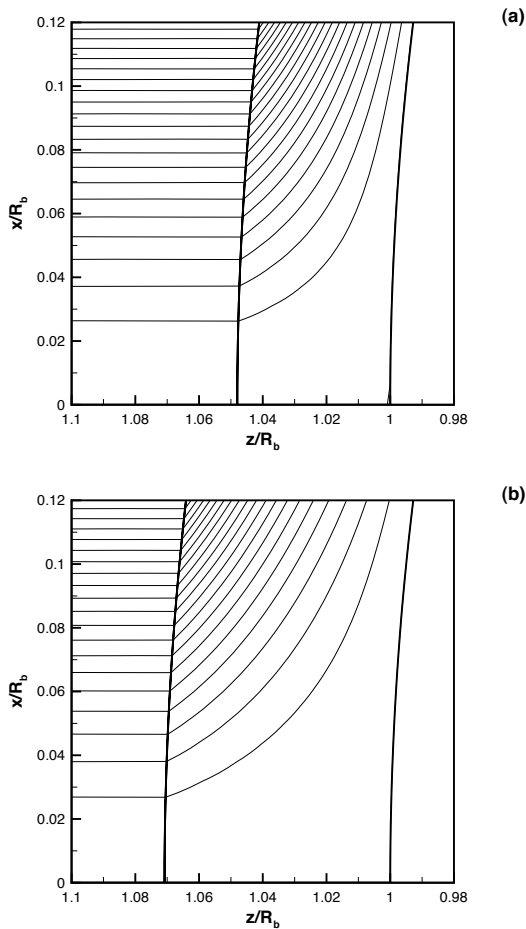
Fig. 2   Effect at $\mathrm{Ma}_\infty = 25$ **of magnetic control on streamlines,** ψ**; contour interval** 2×10^{-5}**. (a) Undisturbed flow. (b) Applied field of** $B_{g0} = 0.86$ **T.**

Fig. 3   Applied field of $B_{g0} = 0.86$ **T at** $\mathrm{Ma}_\infty = 25$**. (a) Magnetic field lines,** $M(r)\sin^2\theta$**; contour interval** 10^{-3}**. (b) Current distribution,** $J_\phi/\sigma V_\infty B_0$**; contour interval** 10^{-2}**.**

Lighthill.[49–51] The flow pattern is similar to the classic incompressible flow stagnation point solution, with an additional acceleration of the fluid around the curve of the body. With the application of a strong magnetic field (0.86 T or $Q_g = 11.4$), there is a dramatic increase in the shock standoff, but little qualitative change in the flow pattern.

Plots of the nondimensional magnetic field and nondimensional current are shown in Fig. 3. For the present case, the induced magnetic field is relatively small, so that the magnetic field lines, Fig. 3a, follow the imposed dipole field closely. At higher values of the magnetic Reynolds number, the magnetic field lines tend to be bent toward the centerline. The corresponding current distribution is shown in Fig. 3b; the vector is directed out of the page. The current increases away from the stagnation streamline, corresponding to the increasing angle, along that direction, between the velocity vector and the magnetic field vector.

One of the important conclusions of the non-magnetic constant density theory is that the flow in the vicinity of the nose of a blunt body is a func-
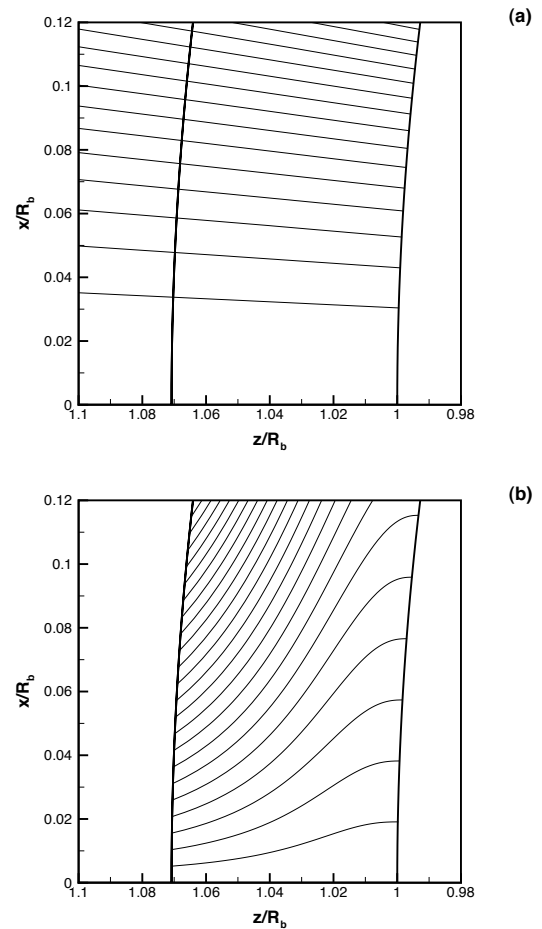
tion of geometry and the shock density ratio only, and is independent of the detailed thermodynamics and chemistry of the shock wave. Thus, for example, the shock standoff distance can be expressed as: $\Delta/R_b = f(K)$. In the magnetogasdynamic case, the parameters Q_g and Re_m^* must be also be considered.

The shock standoff predicted by the inviscid-flow theory is shown in Fig. 4a. To illustrate the influence of magnetic Reynolds number, two cases are shown: one corresponding to the example case discussed previously, and other corresponding to a body twice as large. The shock standoff increases rapidly with the interaction parameter Q_g, with a relatively weak effect of the magnetic Reynolds number.

Since the magnetic force tends to oppose flow across the magnetic field lines, the effect of the applied field is to slow the flow. This effect is illustrated in Fig. 4b, which shows a significant reduction in the stagnation point velocity gradient, determined from Eq. (33), with increasing field strength.

In a non-magnetic flow, a reduction in the magnitude of the stagnation point velocity gradient would
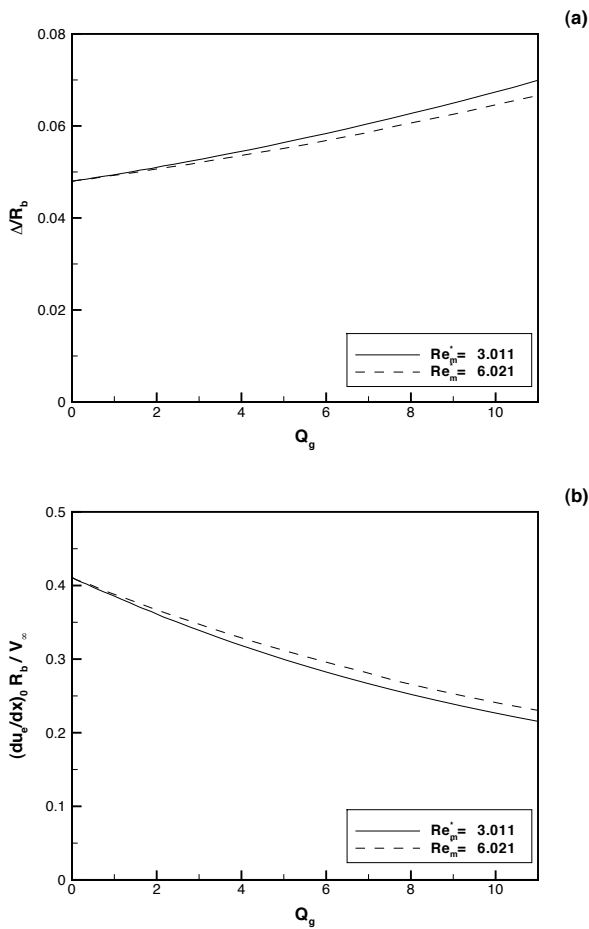
Fig. 4 Effect of varying magnetic field strength at $Ma_\infty = 25$. (a) Shock standoff. (b) Stagnation point velocity gradient.
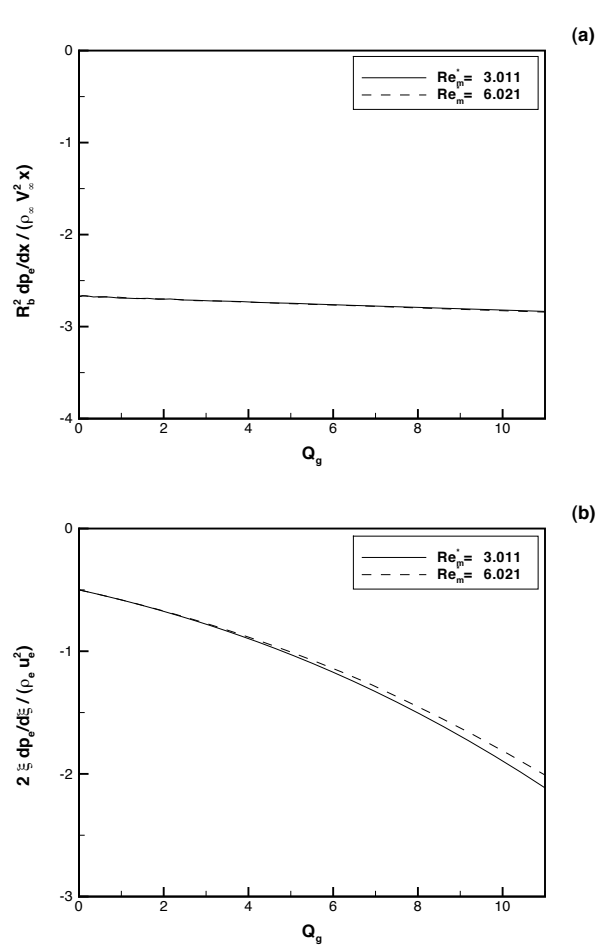

Fig. 5 Effect of varying magnetic field strength on wall pressure gradient at $Ma_\infty = 25$. (a) Outer flow nondimensionalization. (b) Boundary layer nondimensionalization.
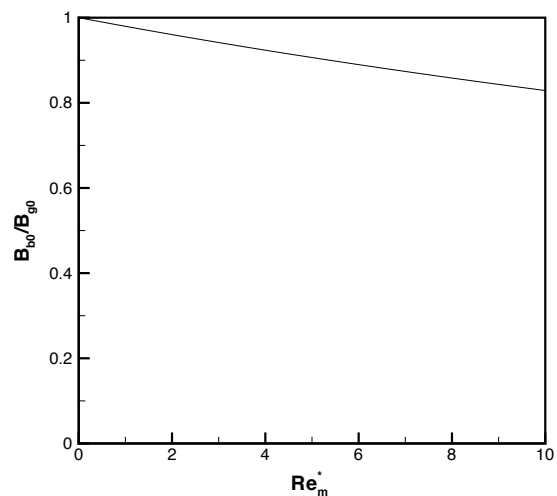
imply a reduction in the magnitude of the pressure gradient. This is not true in the present case, as illustrated in Fig. 5. The stagnation point pressure gradient is negative (favorable), and increasing the strength of the applied field increases the magnitude of the pressure gradient, because the pressure must force the fluid across the magnetic field lines to go around the sphere.

The change in pressure gradient is not very strong relative to the outer flow variables, Fig. 5a, but with the reduction in the boundary layer edge velocity, the relative effect in the boundary layer is strong, Fig. 5b.

The magnetic Reynolds number is seen in Figs. 4-5 to have a modest effect on the flow, generally tending to reduce the effectiveness of magnetic control. This is a consequence of Lenz's law: when a conducting material moves through a magnetic field, currents set up in the conductor generate an induced field that tends to oppose the applied field. Figure 6 shows the ratio of the total magnetic field to the applied field at the nose of the body. With increasing magnetic Reynolds number, the induced field becomes stronger, reducing the overall field and thus the effectiveness of magnetic
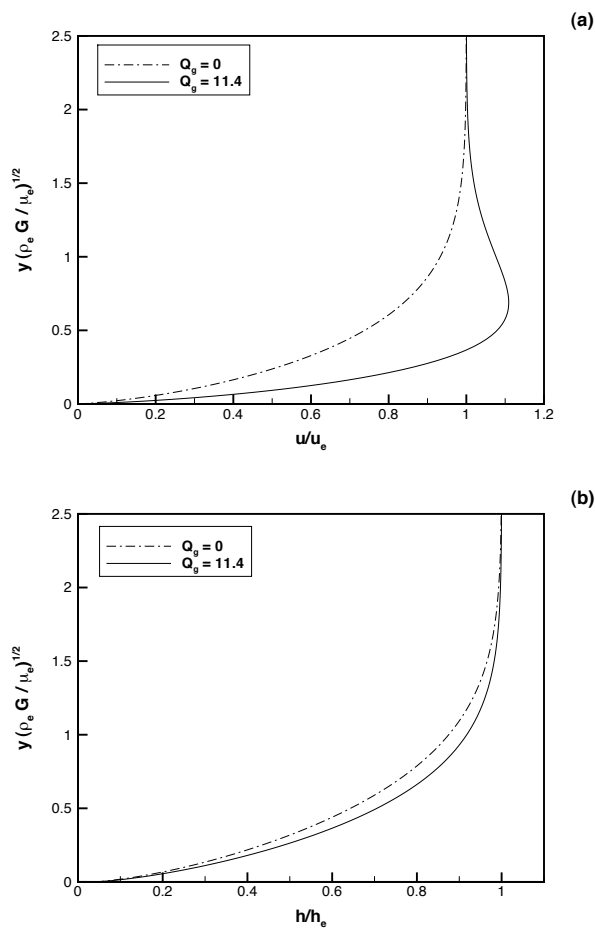

Fig. 6 Effect of magnetic Reynolds number at $Q_g = 11.4$.

Fig. 7 Profiles through the stagnation point boundary layer. (a) Nondimensional velocity. (b) Nondimensional enthalpy.

Fig. 8 Profiles through the stagnation point boundary layer at $x = 0.05$ m. (a) Dimensional velocity. (b) Dimensional temperature.

control.

Example boundary layer profiles are shown in Fig. 7 in nondimensional coordinates. In these coordinates, magnetic control appears to increase the gradients at the wall. This manner of presenting the data is misleading, however, because the values of G and u_e are not the same in the two cases: the freestream is substantially slower with magnetic control. The corresponding dimensional profiles in Fig. 8 show that the dimensional gradients are actually reduced with flow control. Figure 8 also shows that the stagnation point boundary layer thickness is an order of magnitude smaller than the shock standoff distance (Fig. 4), which justifies the use of boundary layer theory.

One interesting feature of the boundary layer solutions is the appearance of overshoot profiles under some conditions. The presence of an inflection point in such a profile should lead to an inviscid instability and promote transition, possibly eliminating the desired reduction in heat transfer. The overshoot profiles are the result of the competing effects of the favorable pressure gradient, which tends to accelerate the flow in the boundary layer, and the magnetic force, which
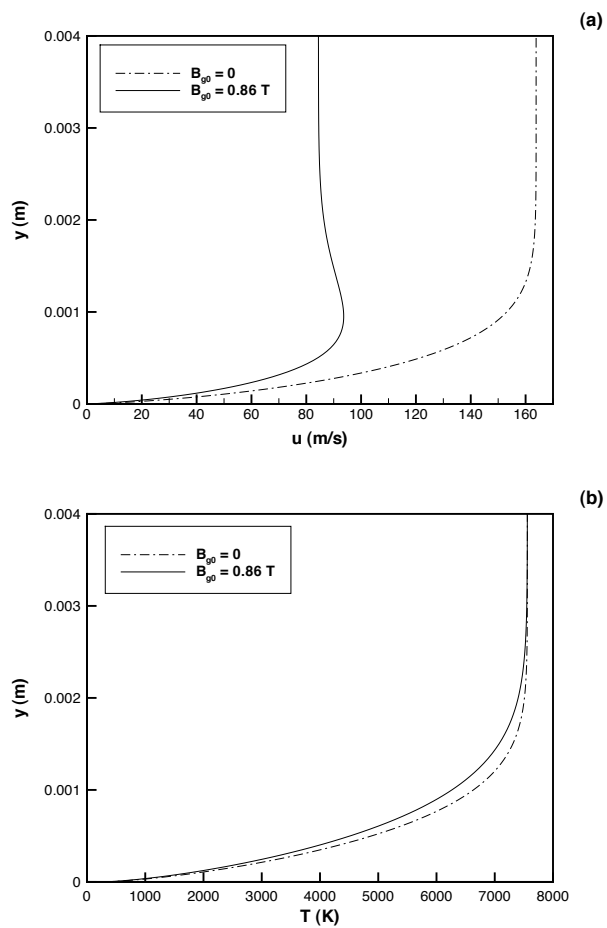
tends to retard the flow. The electrical conductivity falls off with the reduced temperatures near a cold wall, so the effects of the pressure gradient predominate in that region. The magnetic force is stronger near the boundary layer edge. Thus the jet-like feature appears near the middle of the boundary layer. Bush[9] found, using an asymptotic expansion, that the overshoot profiles occur for a cold wall when $nQ_v > 1$ (where $\sigma \propto T^n$).

Calculations (for the sake of brevity, not shown) were also carried out with uniform electrical conductivity, or $n = 0$. In this case no overshoot profiles were found, as predicted by Bush's analysis, and a significantly greater reduction in the wall gradients was obtained.

These results are quantified in Fig. 9, which shows the heat transfer and skin friction relative to the case with no imposed magnetic field. In each plot two curves are shown: one corresponding to a baseline case of variable electrical conductivity ($n = 4.1$), and the other corresponding to constant conductivity ($n = 0$). In all cases, increasing the strength of the imposed magnetic field significantly decreases the skin friction
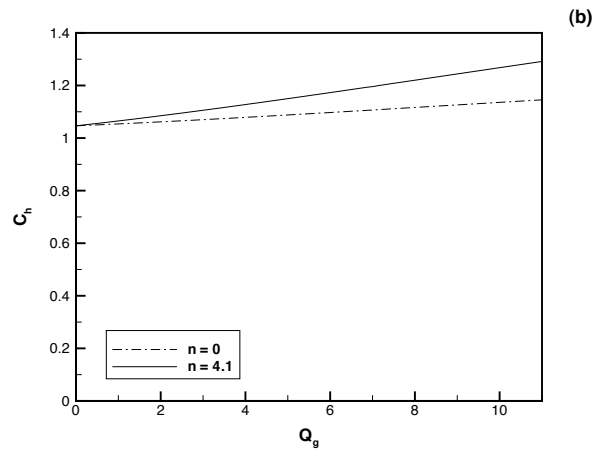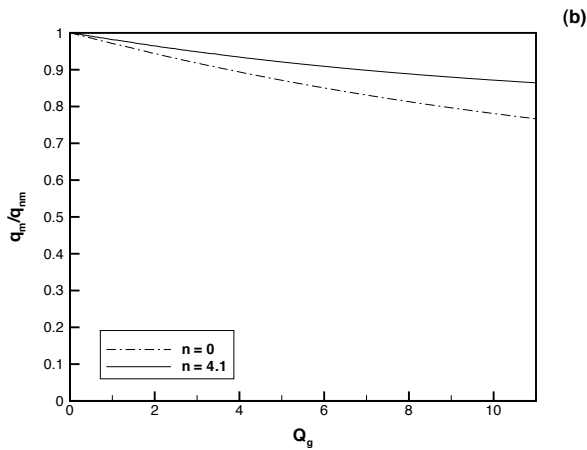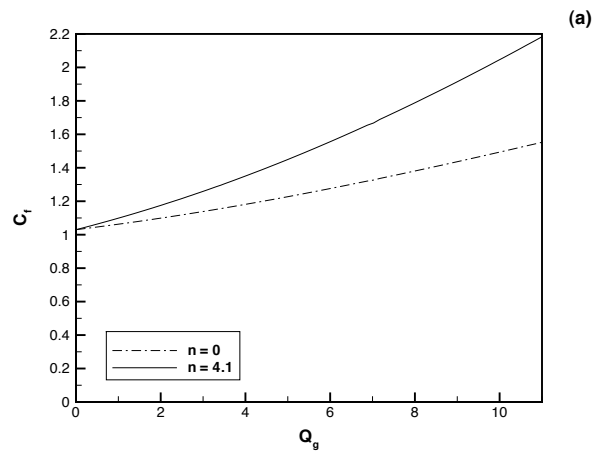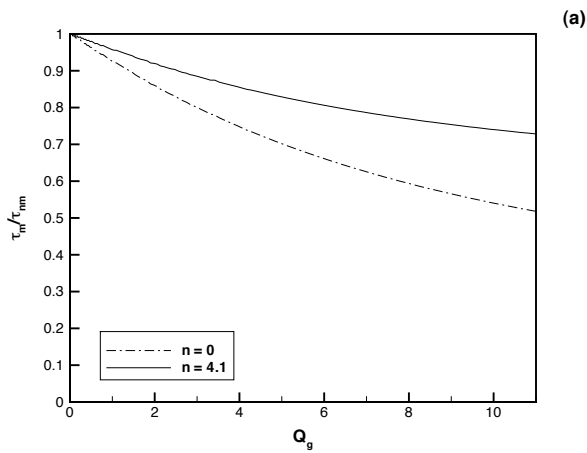
Fig. 9   Effect of magnetic control at the stagnation point. (a) Skin friction. (b) Heat transfer.

Fig. 10   Effect of magnetic control at the stagnation point. (a) Skin friction coefficient. (b) Heat transfer coefficient.

and heat transfer relative to the non-magnetic flow. A substantially greater effect of magnetic control is seen in the uniform conductivity case.

As with the nondimensional profiles in Fig. 7, plots of the traditional boundary layer skin friction coefficient and heat transfer coefficient shown in Fig. 10 give the false impression that magnetic control increases the wall fluxes. The apparent increase is due to the decrease in the edge velocity gradient, G, used to nondimensionalize the fluxes. In the context of the nondimensional boundary layer coordinates, the increase in the nondimensional pressure gradient produces fuller boundary layer profiles (Fig. 7), and increases the relative skin friction and heat transfer. With uniform conductivity (dash-dot lines in Fig. 10), the magnetic force in the boundary layer is better able to resist the pressure gradient, and this effect is reduced.

Numerical Studies

A number of assumptions were required to obtain an analytical solution for the magnetically-controlled blunt body flow. In particular, the constant density assumption, the imposition of a spherical shock wave shape, and geometrical constraints limit the general-

ity of the solution. Numerical simulation of the full magnetogasdynamic equations provides an alternative approach which does not require these restrictive assumptions. We now describe a preliminary effort directed at obtaining the blunt body solution with a direct numerical simulation.

The present effort differs from those those of other research groups[57] in that we consider the non-ideal equations, including Joule heating terms arising out of finite conductivity. We also avoid imposing a magnetic field at the far-field boundary, an unrealistic boundary condition in the frame of reference of a moving aerospace vehicle. Rather, the field is imposed on the surface of the body and is allowed to diffuse and convect into the flow. This situation corresponds more closely to that which could be obtained in an actual flight test.

For simplicity, the flow is assumed in these preliminary computations to be inviscid and thermally non-conducting. The primary mechanism examined is thus the interaction between the inertial and magnetic stresses. As another simplification, the electrical conductivity has been assumed to be constant.

We write the governing equations of non-ideal magnetogasdynamics in terms of non-dimensional quantities normalized by $\rho_{\rm ref}$, $V_{\rm ref}$, a length scale L, $B_{\rm ref}$, and $\sigma_{\rm ref}$. In terms of the non-dimensional variables:

$$
\begin{aligned}
t^* &= \tfrac{tL}{V_{\rm ref}} & \nabla^* &= \tfrac{1}{L}\nabla \\
\vec{v}^* &= \tfrac{\vec{v}}{V_{\rm ref}} & \vec{B}^* &= \tfrac{\vec{B}}{B_{\rm ref}} \\
\rho^* &= \tfrac{\rho}{\rho_{\rm ref}} & p^* &= \tfrac{p}{\rho_{\rm ref}V_{\rm ref}^2} \\
e^* &= \tfrac{e}{V_{\rm ref}^2} & \sigma^* &= \tfrac{\sigma}{\sigma_{\rm ref}}
\end{aligned}
\tag{50}
$$

the governing equations, (7)-(9), become:

$$
\frac{\partial \rho^*}{\partial t^*} + \nabla^* \cdot (\rho^* \vec{v}^*) = 0 \tag{51}
$$

$$
\frac{\partial (\rho^* \vec{v}^*)}{\partial t^*} + \nabla^* \cdot \left[\rho^* \vec{v}^* \vec{v}^* + P^* \mathbf{I} - R_b \vec{B}^* \vec{B}^* \right] = 0 \tag{52}
$$

$$
\frac{\partial Z^*}{\partial t^*} + \nabla^* \cdot \Big[(Z^* + P^*)\vec{v}^* - R_b(\vec{B}^* \cdot \vec{v}^*)\vec{B}^* +
$$
$$
\frac{R_b}{{\rm Re}_m \sigma^*} \left((\vec{B}^* \cdot \nabla^*)\vec{B}^* - (\nabla^* \vec{B}^*) \cdot \vec{B}^* \right) \Big] = 0 \tag{53}
$$

and the induction equation, (6), is:

$$
\frac{\partial \vec{B}^*}{\partial t^*} + \nabla^* \cdot \left(\vec{v}^* \vec{B}^* - \vec{B}^* \vec{v}^* \right) +
$$
$$
\frac{1}{{\rm Re}_m} \nabla^* \times \left[\frac{1}{\sigma^*} \nabla^* \times \vec{B}^* \right] = 0 \tag{54}
$$

We have introduced the parameters:

$$
P^* = p^* + R_b \frac{(B^*)^2}{2} \tag{55}
$$

$$
Z^* = \rho^* e^* + \frac{\rho^* (v^*)^2}{2} + R_b \frac{(B^*)^2}{2} \tag{56}
$$

$R_b = B_{\rm ref}^2/[\rho_{\rm ref}U_{\rm ref}^2\mu_0]$ is the magnetic force (or pressure) number and ${\rm Re}_m = LU_{\rm ref}\mu_0\sigma_{\rm ref}$ is the magnetic Reynolds number. For convenience, the superscript (*) will be dropped in subsequent discussions of the numerical computations, and all quantities will be assumed to be non-dimensional unless explicitly otherwise stated.

The governing equations are solved by first writing the flux-vector form of the governing equations in general curvilinear (ξ, η, ζ) coordinates.[46,58] Each derivative in transformed space $(\Delta\xi = \Delta\eta = \Delta\zeta = 1)$ is approximated with a standard second-order centered formula:

$$
\frac{\partial \phi}{\partial \xi} = \frac{\phi_{i+1} - \phi_{i-1}}{2} \tag{57}
$$

In order to enforce stability, a popular second- and fourth-order blend of damping[59] was extended to the magnetogasdynamics equations by adding terms pertinent to the induction equation in a straightforward fashion. A steady state is assumed to exist and is obtained by evolving the governing equations in time
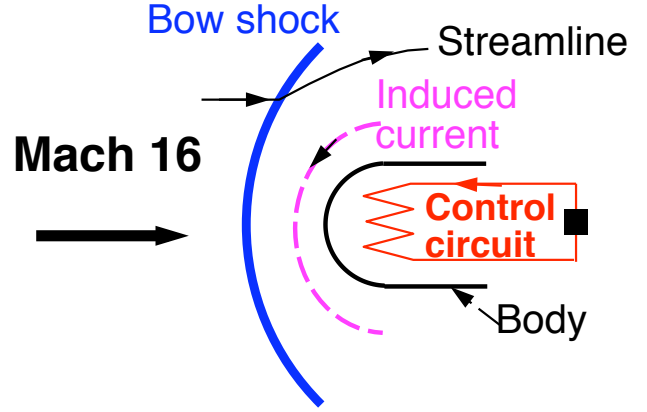

Fig. 11   Configuration for numerical computations.

with a standard four-stage Runge-Kutta method[60] enhanced with local time-stepping techniques to improve the convergence rate.

The configuration for the problem is depicted in Fig. 11. A cylindrical body is placed in an incoming Mach 16 flow. The source of the imposed field is assumed to be an electrical circuit located inside the body. The circuit is assumed to be "compensated," in the sense that B_z is the only field component. B_x and B_y are zero in the initial condition and, for this two-dimensional case in which the velocity vector lies in the x-y plane, it is straightforward to show that these components remain zero at all times. Thus, $B_x = B_y = 0$ and $B_z = B_z(x,y)$. The B_z field is assumed to decay to zero at the far-field boundary, and simple extrapolation and symmetry conditions are applied at the downstream and symmetry boundaries, respectively.

In specifying the value of B_z at the surface, we take an approach similar to that of Bush, and assume that the net field due to the effects of the electrical circuit and the induced currents (which, due to the geometrical arrangement of the B- and v-fields lie in the $x - y$ plane) is such as to yield $B_z = 1$ on the surface. If required, the precise nature of the control circuit can be determined afterwards.

The imposed E-field is assumed to be zero. Induced E-fields arise during transients but decay as the steady state is approached. The fluid dynamic boundary conditions are straightforward: the incoming flow field is specified, symmetry is assumed along the stagnation line, and zero gradient is assumed at the downstream end of the domain. The normal velocity at the cylinder surface is set to zero, and the tangential velocity is extrapolated from the interior. The surface pressure is determined by satisfying $\partial P/\partial n = 0$.

Although this approach is one of several well-posed techniques of specifying the boundary conditions at the body surface, it can nevertheless yield unphysical negative surface pressures due to over-expansion near the shoulder, when the magnetic interaction parameter is large. To address this problem, the B-field is allowed to diminish, such that the surface pressure al-
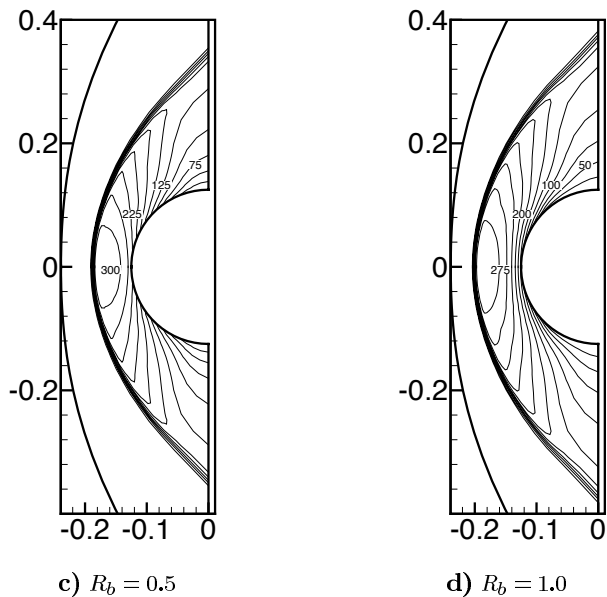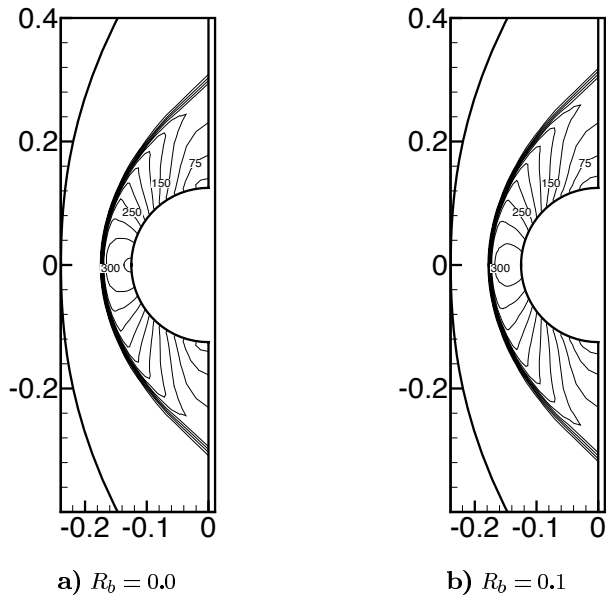
a) $R_b = 0.0$

b) $R_b = 0.1$

c) $R_b = 0.5$

d) $R_b = 1.0$

Fig. 12   Pressure contours.

Fig. 13   Surface pressure; every fourth point marked with symbol.
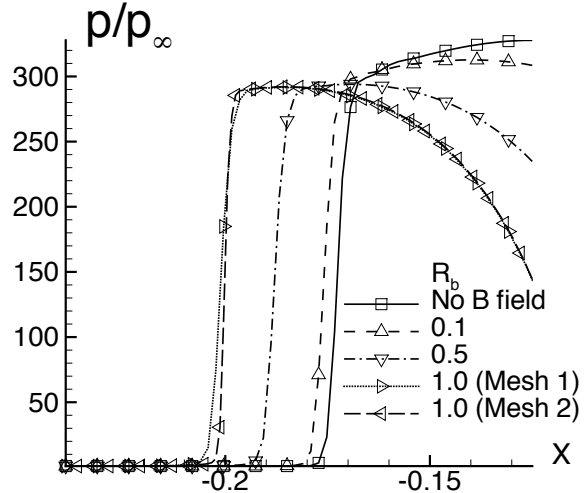
Fig. 14   Static pressure along stagnation streamline; every fourth point marked with symbol.

ways exceeds $0.5p_{\mathrm{ref}}$. Note that the imposition of a B-field large enough to yield near-vacuum conditions is precluded in a viscous flow by the appearance of phenomena such as flow separation, which redistribute the velocity field and limit the drop in pressure. Since viscous forces are ignored in the present work, it is necessary to reduce the B-field near the shoulder as specified above.

Features of the pressure field are shown in Figs. 12-14, for a magnetic Reynolds number of $Re_\sigma = 100$, and for several values of the interaction parameter: $R_b = 0.1$, 0.5 and 1.0. The quantity plotted is $p/p_\infty = p^* \gamma M_\infty^2$, where $M_\infty = 16$ is the freestream Mach number.

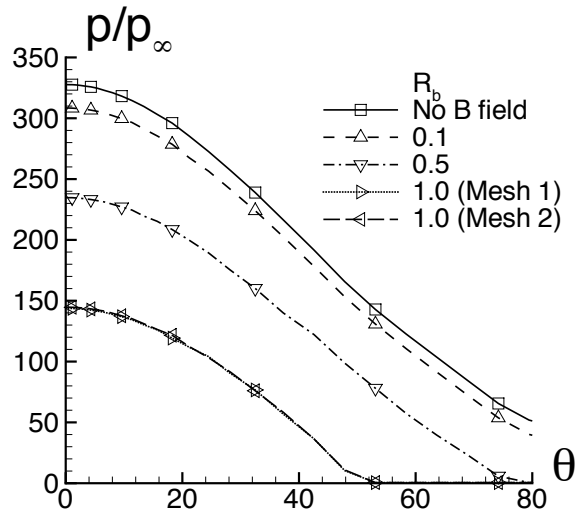The overall features of the pressure field re-main qualitatively similar at all interaction strengths (Fig. 12). The shock standoff is seen to increase continuously with increasing interaction parameter. Although the pressure contours assume orientations increasingly aligned with the body surface as the interaction parameter R_b is increased, no new clearly identifiable features appear in the field.

A more quantitative assessment is presented in Figs. 13-14 which depict the static pressure along the body surface and stagnation streamline, respectively. In each figure, the solution without any magnetic interaction is plotted, along with surface pressures at various interaction parameters. For the largest interaction case ($R_b = 1$), the solution is plotted on two meshes of 35×61 and 35×121 points. These solutions suggest that mesh independence has been

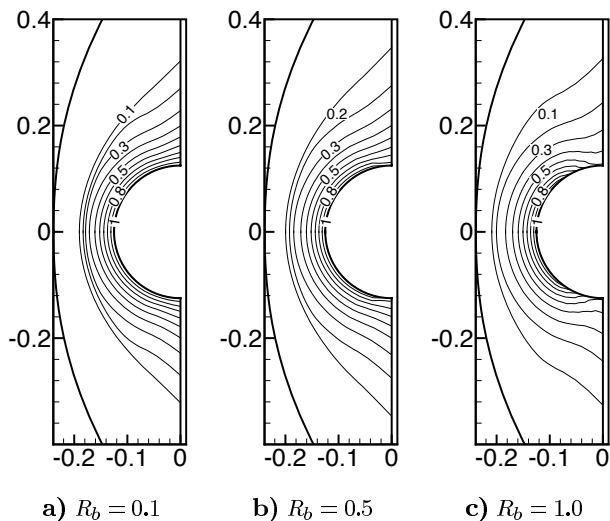a) $R_b = 0.1$ b) $R_b = 0.5$ c) $R_b = 1.0$

Fig. 15   Contours of magnetic field strength.
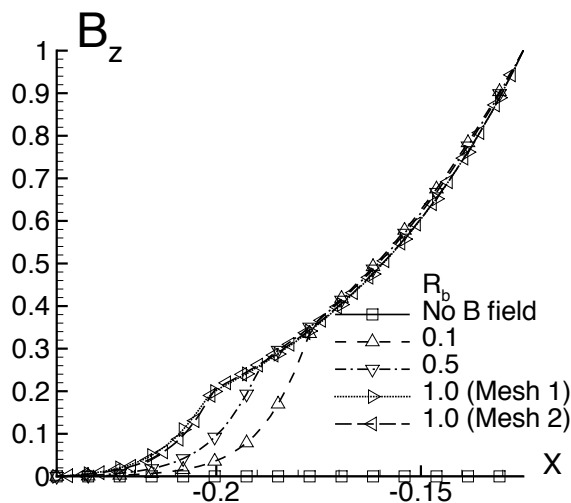

Fig. 16   Magnetic field along stagnation streamline.

achieved; ongoing computations are focused on increasing streamwise spacing as well.

The static pressure on the entire surface drops substantially with increasing magnetic interaction parameter. Note, however, that for $R_b = 0.5$ and 1.0, the pressure around the shoulder is prevented from dropping below $0.5p_\infty$ by reducing the surface magnetic field. In the absence of a magnetic field, the pressure rise at the surface $p_{b0}/p_\infty \approx 330$ is consistent with the anticipated value from theory as obtained with the Rayleigh supersonic Pitot formula.[61]

Figure 14 shows that, even though the shock standoff distance increases, the strength of the shock, measured in terms of the pressure ratio across it, is not diminished perceptibly due to the imposition of the magnetic field. This observation is consistent with the features of the magnetic field shown in Figs. 15-16. The magnetic field is highest near the surface and de-

cays away from the body. It is relatively small near the shock location, and thus has minimal impact on the shock pressure ratio. The region of significant magnetic field strength increases with the interaction parameter. Although the non-dimensional gradient of B_z increases with a drop in the interaction parameter, it is important to note that the dimensional current is also proportional to the reference value of B, which diminishes with interaction parameter. In the limit of $R_b = 0$, the magnetic field has no impact on the fluid dynamics, but persists as an essentially passive vector field, convected, stretched, and diffused according to the induction equation.

Finally, the total drag on the body is dependent not only on the static pressure, but also on the magnetic pressure. A preliminary computation suggests that no perceptible change is obtained in terms of overall *forebody* drag. Since the surface magnetic field is known ($B_z = 1$), a straightforward calculation of the term $0.5\gamma M^2 R_b B_{\text{surface}}^2/\mu_0$ yields a value of $179.2R_b$, which, when added to the plotted static pressure, yields similar sums of static and magnetic pressures, regardless of the interaction parameter. An assessment of the change in drag for an overall aerospace configuration cannot as yet be performed, because the impact of the magnetic field on the base region has not been considered in this work.

Conclusions

The possibility of magnetic control of hypersonic blunt body flows was explored theoretically and computationally. A theoretical model, due to W. B. Bush,[6,9] of hypersonic flow over an axisymmetric, spherical-nose body with an imposed dipole field was reviewed. A preliminary computational study of the flow over a two-dimensional cylinder configuration with magnetic control was carried out employing a new, non-ideal, magnetogasdynamics code. Using an inviscid model for the outer flow, both the theory and the computations show than an applied magnetic field can slow the flow in the shock layer. Boundary layer theory predicts a reduction in the stagnation point heat transfer.

The effectiveness of control was found to be sensitive to the electrical conductivity of the ionized air in the shock layer. Magnetic field strengths on the order of 1 T (10^4 G) or higher are needed for electrical conductivities corresponding to the natural levels of ionization present in typical re-entry flows ($\sim 10^2/(\Omega\text{-m})$). Higher conductivity allows correspondingly lower magnetic field strengths to achieve the same level of control. (Although increasing the conductivity increases the deleterious effects of the induced field that come with increased magnetic Reynolds number, the effect through the interaction parameter is very much greater, and there is a strong net gain for increased electrical conductivity.) More uniform conductivity

also improves the effectiveness of magnetic control, and mitigates the tendency of the stagnation point boundary layer to develop overshoot velocity profiles.

The electrical conductivity in the shock layer could be augmented through artificial ionization. Various forms of energy addition, such as microwave discharges and electron beams, have been considered elsewhere for this purpose. It will be necessary to develop computational tools to study the engineering tradeoffs associated with these techniques.

Acknowledgments

References

[1]Kantrowitz, A. R., "A Survey of Physical Phenomena Occurring in Flight at Extreme Speeds," *Proceedings of the Conference on High-Speed Aeronautics*, edited by A. Ferri, N. J. Hoff, and P. A. Libby, Polytechnic Institute of Brooklyn, New York, 1955, pp. 335–339.

[2]Resler, E. L. and Sears, W. R., "The Prospects for Magneto-Aerodynamics," *Journal of the Aeronautical Sciences*, Vol. 25, No. 4, 1958, pp. 235–245,258.

[3]Resler, E. L. and Sears, W. R., "The Prospects for Magneto-Aerodynamics – Correction and Addition," *Journal of the Aero/Space Sciences*, Vol. 26, No. 5, 1959, pp. 318.

[4]Sears, W. R., "Magnetohydrodynamic Effects in Aerodynamic Flows," *American Rocket Society Journal*, Vol. 29, No. 6, 1959, pp. 397–406.

[5]Ziemer, R. W. and Bush, W. B., "Magnetic Field Effects on Bow Shock Stand-off Distance," *Physical Review Letters*, Vol. 1, No. 2, 1958, pp. 58–59.

[6]Bush, W. B., "Magnetohydrodynamic-Hypersonic Flow Past a Blunt Body," *Journal of the Aero/Space Sciences*, Vol. 25, No. 11, 1958, pp. 685–690,728.

[7]Bush, W. B., "A Note on the Magnetohydrodynamic-Hypersonic Flow Past a Blunt Body," *Journal of the Aero/Space Sciences*, Vol. 26, No. 8, 1959, pp. 536–537.

[8]Bush, W. B., "Compressible Flat-Plate Boundary-Layer Flow With an Applied Magnetic Field," *Journal of the Aero/Space Sciences*, Vol. 27, No. 1, 1960, pp. 49–58.

[9]Bush, W. B., "The Stagnation-Point Boundary Layer in the Presence of an Applied Magnetic Field," *Journal of the Aerospace Sciences*, Vol. 28, No. 8, 1961, pp. 610–611,630.

[10]Ziemer, R. W., "Experimental Investigation in Magneto-Aerodynamics," *American Rocket Society Journal*, Vol. 29, No. 9, 1959, pp. 642–647.

[11]Kemp, N. H., "On Hypersonic Stagnation-Point Flow with a Magnetic Field," *Journal of the Aeronautical Sciences*, Vol. 25, No. 6, 1958, pp. 405–407.

[12]Freeman, N. C., "On the Flow Past a Sphere at Hypersonic Speed With a Magnetic Field," *Journal of the Aero/Space Sciences*, Vol. 26, No. 10, 1959, pp. 670–672.

[13]Kemp, N. H., "Author's Reply," *Journal of the Aero/Space Sciences*, Vol. 26, No. 10, 1959, pp. 670–672.

[14]Kemp, N. H., "Hydromagnetic Effects on Heating and Shear at a Three-Dimensional Stagnation Point in Hypersonic Flow," *Journal of the Aero/Space Sciences*, Vol. 27, No. 7, 1960, pp. 553–554.

[15]Lykoudis, P. S., "The Newtonian Approximation in Magnetic Hypersonic Stagnation-Point Flow," *Journal of the Aerospace Sciences*, Vol. 28, No. 7, 1961, pp. 541–546,562.

[16]Neuringer, J. L. and McIlroy, W., "Incompressible Two-Dimensional Stagnation-Point Flow of an Electrically Conducting Viscous Fluid in the Presence of a Magnetic Field," *Journal of the Aeronautical Sciences*, Vol. 25, No. 3, 1958, pp. 194–198.

[17]Neuringer, J. L. and McIlroy, W., "Hydromagnetic Effects on Stagnation-Point Heat Transfer," *Journal of the Aeronautical Sciences*, Vol. 25, No. 5, 1958, pp. 332–334.

[18]Rossow, V. J., "On Flow of Electrically Conducting Fluids Over a Flat Plate in the Presence of a Transverse Magnetic Field," NACA Technical Note 3971, National Advisory Committee for Aeronautics, Washington, DC, May 1957.

[19]Rossow, V. J., "Magnetohydrodynamic Analysis of Heat Transfer Near a Stagnation Point," *Journal of the Aeronautical Sciences*, Vol. 25, No. 5, 1958, pp. 334–335.

[20]Meyer, R. X., "Magnetohydrodynamics and Aerodynamic Heating," *American Rocket Society Journal Journal*, Vol. 29, No. 3, 1959, pp. 187–192.

[21]Meyer, R. C., "On Reducing Aerodynamic Heat-Transfer Rates by Magnetohydrodynamic Techniques," *Journal of the Aero/Space Sciences*, Vol. 25, No. 9, 1958, pp. 561–566,572.

[22]Lykoudis, P. S., "The Matching of the Viscid and Inviscid Regions for the Stagnation Magnetic Flow," *Journal of the Aero/Space Sciences*, Vol. 26, No. 5, 1959, pp. 315–317.

[23]Seeman, G. R. and Cambel, A. B., "Observations Concerning Magnetoaerodynamic Drag and Shock Standoff Distance," *Proceedings of the National Academy of Sciences*, Vol. 55, No. 3, 1966, pp. 457–465.

[24]Porter, R. W. and Cambel, A. B., "Magnetic Coupling in Flight Magnetoaerodynamics," *AIAA Journal*, Vol. 5, No. 4, 1967, pp. 803–805.

[25]Nowak, R., Kranc, S., Porter, R. W., Yuen, M. C., and Cambel, A. B., "Magnetogasdynamic Re-Entry Phenomena," *Journal of Spacecraft and Rockets*, Vol. 4, No. 11, 1967, pp. 1538–1542.

[26]Kranc, S., Yuen, M. C., and Cambel, A. B., "Experimental Investigation of Magnetoaerodynamic Flow Around Blunt Bodies," NASA Contractor Report 1393, National Aeronautics and Space Administration, Washington, DC, August 1969.

[27]Wu, C.-S., "Hypersonic Viscous Flow Near the Stagnation Point in the Presence of Magnetic Field," *Journal of the Aerospace Sciences*, Vol. 27, No. 12, 1960, pp. 882–893,950.

[28]Smith, M. C. and Wu, C.-S., "Magnetohydrodynamic Hypersonic Viscous Flow Past a Blunt Body," *AIAA Journal*, Vol. 2, No. 5, 1964, pp. 963–965.

[29]Smith, M. C., Schwimmer, H. S., and Wu, C.-S., "Magnetohydrodynamic-Hypersonic Viscous and Inviscid Flow Near the Stagnation Point of a Blunt Body," *AIAA Journal*, Vol. 3, No. 7, 1965, pp. 1365–1367.

[30]Porter, R. W. and Cambel, A. B., "Comment on 'Magnetohydrodynamic-Hypersonic Viscous and Inviscid Flow Near the Stagnation Point of a Blunt Body'," *AIAA Journal*, Vol. 4, No. 5, 1966, pp. 952–953.

[31]Smith, M. C., Schwimmer, H. S., and Wu, C.-S., "Reply by Authors to R. W. Porter and A. B. Cambel," *AIAA Journal*, Vol. 4, No. 5, 1966, pp. 953.

[32]Levy, R. H., "A Simple MHD Flow with Hall Effect," *AIAA Journal*, Vol. 1, No. 3, 1963, pp. 698–699.

[33]Porter, R. W. and Cambel, A. B., "Hall Effect in Flight Magnetogasdynamics," *AIAA Journal*, Vol. 5, No. 12, 1967, pp. 2208–2213.

[34]Kranc, S., Porter, R. W., and Cambel, A. B., "Electrodeless Magnetogasdynamic Power During Entry," *Journal of Spacecraft and Rockets*, Vol. 4, No. 6, 1967, pp. 813–815.

[35]Goulard, R., "Optimum Magnetic Field for Stagnation Heat Transfer Reduction at Hypersonic Velocities," *ARS Journal*, Vol. 29, No. 8, 1959, pp. 604–605.

[36]Phillips, R. L., "Effect of Magnetic Drag on Re-Entry Body Heating," *American Rocket Society Journal*, Vol. 31, No. 5, 1961, pp. 672–674.

[37]Ericson, W. B. and Maciulaitis, A., "Investigation of Magnetohydrodynamic Flight Control," *Journal of Spacecraft and Rockets*, Vol. 1, No. 3, 1964, pp. 283–289.

[38]Gurijanov, E. P. and Harsha, P. T., "AJAX: New Directions in Hypersonic Technology," AIAA Paper 96-4609, November 1996.

[39]Hilbun, W. M., *Shock Waves in Nonequilibrium Gases and Plasmas*, Ph.D. thesis, Air Force Institute of Technology, Wright-Patterson AFB, OH, October 1997.

[40]Adamovich, I. V., Subramaniam, V. V., Rich, J. W., and Macheret, S. O., "Phenomenological Analysis of Shock-Wave Propagation in Weakly Ionized Plasmas," *AIAA Journal*, Vol. 36, No. 5, 1998, pp. 816–822.

[41]Shang, J. S., Ganguly, B., Umstattd, R., Hayes, J., Arman, M., and Bletzinger, P., "Developing a Facility for Magneto-Aerodynamic Experiments," AIAA Paper 2000-0447, January 2000.

[42]Poggie, J., "Energy Addition for Shockwave Control," AIAA Paper 99-3612, June 1999.

[43]Poggie, J., "Modeling the Propagation of a Shock Wave through a Glow Discharge," *AIAA Journal*, 2000, to appear; see also AIAA 99-0867.

[44]Josyula, E., "Computational Study of Vibrationally Relaxing Gas Past Blunt Body in Hypersonic Flows," AIAA Paper 99-0866, January 1999.

[45]Josyula, E., "Computational Study of Effect of Oxygen Atoms on Vibrational Relaxation of N_2 in High-Speed Air Flow Past Blunt Body," AIAA Paper 99-4835, November 1999.

[46]Gaitonde, D. V., "Development of a Solver for 3-D Non-Ideal Magnetogasdynamics," AIAA Paper 99-3610, June 1999.

[47]Hughes, W. F. and Young, F. J., *The Electromagnetodynamics of Fluids*, J. Wiley, New York, 1966.

[48]Spitzer, L., *Physics of Fully Ionized Gases*, Interscience Publishers, New York, 2nd ed., 1962.

[49]Hida, K., "An Approximate Study on the Detached Shock Wave in front of a Circular Cylinder and a Sphere," *Journal of the Physical Society of Japan*, Vol. 8, No. 6, 1953, pp. 740–745.

[50]Hida, K., "Supplementary Note to my Paper 'An Approximate Study on the Detached Shock Wave in front of a Circular Cylinder and a Sphere'," *Journal of the Physical Society of Japan*, Vol. 10, No. 1, 1955, pp. 79–81.

[51]Lighthill, M. J., "Dynamics of a Dissociating Gas, Part I: Equilibrium Flow," *Journal of Fluid Mechanics*, Vol. 2, No. 1, 1957, pp. 1–32.

[52]Whitham, G. B., "A Note on the Stand-off Distance of the Shock in High Speed Flow Past a Circular Cylinder," *Communications on Pure and Applied Mathematics*, Vol. 10, No. 4, 1957, pp. 531–535.

[53]Hayes, W. D. and Probstein, R. F., *Hypersonic Flow Theory*, Academic Press, New York, 1st ed., 1959.

[54]Ambrosio, A. and Wortman, A., "Stagnation Point Shock Detachment Distance for Flow Around Spheres and Cylinders," *ARS Journal*, Vol. 32, No. 2, 1962, pp. 281.

[55]de Hoffmann, F. and Teller, E., "Magneto-Hydrodynamic Shocks," *Physical Review*, Vol. 80, No. 4, 1950, pp. 692–703.

[56]Plooster, M. N., "Numerical Simulation of Spark Discharges in Air," *The Physics of Fluids*, Vol. 14, No. 10, 1971, pp. 2111–2123.

[57]Damevin, H.-M., Hoffmann, K. A., and Dietiker, J.-F., "Numerical Simulation of Hypersonic MHD Applications," AIAA Paper 99-3611, June 1999.

[58]Anderson, D. A., Tannehill, J. C., and Pletcher, R. H., *Computational Fluid Mechanics and Heat Transfer*, Hemisphere Publishing, New York, 1st ed., 1984.

[59]Jameson, A., Schmidt, W., and Turkel, E., "Numerical Solutions of the Euler Equations by a Finite Volume Method Using Runge-Kutta Time Stepping Schemes," AIAA Paper 81-1259, 1981.

[60]Conte, S. and de Boor, C., *Elementary Numerical Analysis: An Algorithmic Approach*, McGraw-Hill, New York, 1980.

[61]Ames Research Staff, "Equations, Tables, and Charts for Compressible Flow," NACA Report 1135, Ames Aeronautical Laboratory, National Advisory Commmittee for Aeronautics, Moffett Field, CA, 1953.